Dual-Color Electroluminescence from Dot-in-Bulk Nanocrystals

ARTICLE *in* NANO LETTERS · DECEMBER 2013

Impact Factor: 13.59 · DOI: 10.1021/nl403478s · Source: PubMed

6 AUTHORS, INCLUDING:

Sergio Brovelli
Università degli Studi di Milano-Bicocca
77 PUBLICATIONS **1,318** CITATIONS
SEE PROFILE

Wan Ki Bae
Korea Institute of Science and Technology
54 PUBLICATIONS **1,534** CITATIONS
SEE PROFILE

Umberto Giovanella
Italian National Research Council
67 PUBLICATIONS **848** CITATIONS
SEE PROFILE

Francesco Meinardi
Università degli Studi di Milano-Bicocca
189 PUBLICATIONS **2,752** CITATIONS
SEE PROFILE

NANO LETTERS

Letter

pubs.acs.org/NanoLett

Dual-Color Electroluminescence from Dot-in-Bulk Nanocrystals

Sergio Brovelli,*[,†] Wan Ki Bae,[‡] Christophe Galland,[‡,§] Umberto Giovanella,[∥] Francesco Meinardi,[†] and Victor I. Klimov*[,‡]

[†]Dipartimento di Scienza dei Materiali, Università degli Studi di Milano-Bicocca, via Cozzi 55, I-20125 Milano, Italy

[‡]Chemistry Division, Los Alamos National Laboratory, Los Alamos, New Mexico 87545, United States

[§]École Polytechnique Fédérale de Lausanne (EPFL), CH-1015, Lausanne, Switzerland

[∥]Istituto per lo Studio delle Macromolecole (ISMac-CNR), via Bassini 15, Milano 20133, Italy

Supporting Information

ABSTRACT: The emission color from colloidal semiconductor nanocrystals (NCs) is usually tuned through control of particle size, while multicolor emission is obtained by mixing NCs of different sizes within an emissive layer. Here, we demonstrate that recently introduced "dot-in-bulk" (DiB) nanocrystals can emit two-color light under both optical excitation and electrical injection. We show that the effective emission color can be controlled by adjusting the relative amplitudes of the core and shell emission bands via the intensity of optical excitation or applied bias in the cases of photoluminescence (PL) and electroluminescence (EL), respectively. To investigate the role of nonradiative carrier losses due to trapping at intragap states, we incorporate DiB NCs into functional light-emitting diodes and study their PL as a function of applied bias below the EL excitation threshold. We show that voltage-dependent changes in core and shell emissions are not due to the applied electric field but rather arise from the transfer of charges between the anode and the NC intragap trap sites. The changes in the occupancy of trap states can be described in terms of the raising (lowering) of the Fermi level for reverse (direct) bias. We find that the applied voltage affects the overall PL intensity primarily via the electron-trapping channel while bias-induced changes in hole-trapping play a less significant role, limited to a weak effect on core emission.

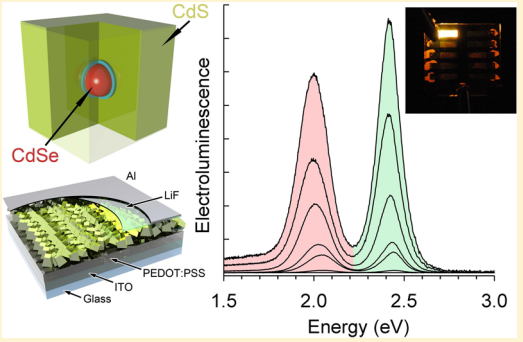

KEYWORDS: *Nanocrystal quantum dot, core/shell heterostructure, dual emission, electroluminescence, light-emitting diode, surface defect*

Colloidal semiconductor nanocrystals (NCs) are color-tunable, solution-processable optical materials with potential applications in light-emitting diodes (LEDs),[1] lasers,[2,3] luminescent markers,[4,5] phosphors,[6] and single photon sources.[7] Typical approach to tuning emission color is through particle size control (that is, control of the confinement contribution to the band gap energy, E_g)[8] and/or hetero-structuring (wave function engineering)[9] exploiting type-I, type-II, or quasi-type-II localization regimes. The combination of CdSe and CdS has been widely used in colloidal heterostructures fabricated as tetrapods,[10] axial dot-in-rod structures,[11] dot-in-plate,[12] and spherical core/shell NCs.[13] One specific architecture, wherein a small CdSe core is overcoated with an exceptionally thick CdS shell ("giant" or g-NCs) has received special attention, as it allows for suppression of photoluminescence (PL) intermittency ("blinking")[14−16] and reduced rates of nonradiative Auger recombination.[17−20] All of these nanostructures are characterized by a large valence band offset at the CdSe/CdS interface and a small energy difference between the conduction band edges. As a result, holes are tightly confined within the CdSe core while the electrons are delocalized over the entire structure. This situation is usually referred to as a quasi-type II confinement regime (Figure 1a).[11,18,21] Because of extremely fast relaxation of holes from the CdS domain of the structure to the core (<1 ps; ref 19), the emission from these NCs is dominated by the recombination of core excitons. Under intense excitation with subpicosecond laser pulses, one can saturate the CdSe core hole states and observe an additional emission band from the CdS region.[18,22,23] This, however, is usually not possible with continuous wave (cw) excitation sources or electrical injection, when the excitation rate is much lower that the rate of Auger recombination involving core-localized holes.

One approach for obtaining dual emission under weak excitation (optical or electrical) is through designing a structure in which relaxation of holes into the core is slowed down to a degree such that holes have a chance to recombine radiatively within the CdS domain of the hetero-NC (Figure 1b). In this way, one should be able to control the relative intensities of core and shell emission by simply changing the generation rate of electron−hole pairs within the shell region (shell-based

Received: September 17, 2013
Revised: December 2, 2013
Published: December 12, 2013

   dx.doi.org/10.1021/nl403478s | *Nano Lett.* 2014, 14, 486−494

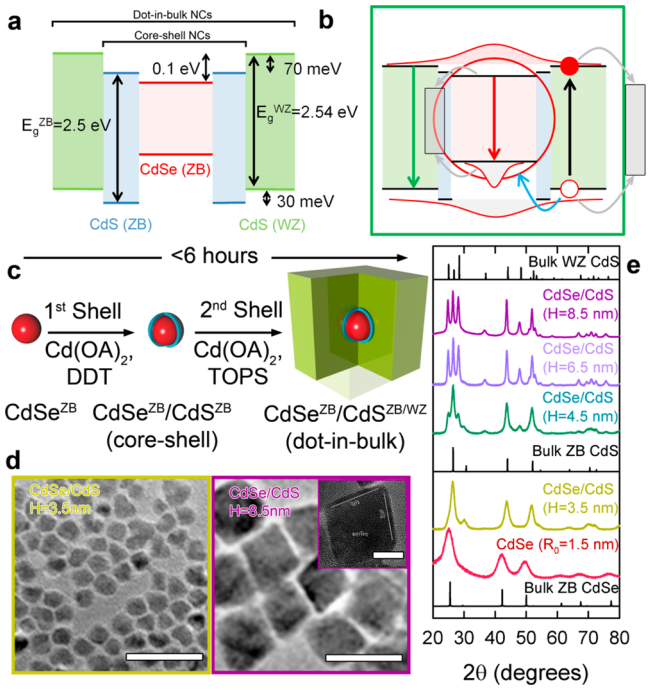

Figure 1. (a) A band alignment diagram of bulk CdSe and CdS showing the difference in the conduction and valence band energies of the ZB and WZ forms of CdS. (b) In DiB NCs, a thin interfacial ZB CdS layer creates a hole blocking barrier which inhibits hole trapping from a thick WZ CdS shell into the CdSe core. Arrows show photoexctation and various relaxation and recombiantion processes. After excitation within the shell region (black arrow), the photogenerated hole can either directly recombine radiatively with a conduction band electron (green arrow) or first relax into the core state (blue arrow) and then recombine with the electron (red arrow). Alternatively, the electron and the hole can be trapped (gray arrows) at intragap defects states located at the core/shell interface or on the NC surface and then recombine with the carrier of the opposite sign. (c) Schematic diagram illustrating the synthesis of DiB CdSe/CdS NCs (see Methods for details and notations). (d) Transmission electron microscopy images of CdSe/CdS NCs with core radius R_0 = 1.5 nm and different shell thicknesses (H = 3.5 and 8.5 nm). Scale bars in the main panels correspond to 40 nm and to 10 nm in the inset at the top of the right panel. (e) X-ray diffraction (XRD) patterns of NCs with R_0 = 1.5 nm and different thicknesses (H = 0, 3.5, 4.5, 6.5, and 8.5 nm) in comparison to the XRD spectra of bulk CdSe and CdS.

excitations dominate the absorption cross-section at photon energies above the CdS band edge). Recently, we demonstrated that this regime can be realized using novel "dot-in-bulk" (DiB) nanostructures where the quantum-confined CdSe core is encapsulated into a thick (7−9 nm), bulklike CdS shell (Figure 1a,b).[24] In that study, we showed that in DiB NCs relaxation of shell holes into the core states is dramatically slowed down compared to other types of reported CdSe/CdS nanostructures. We have attributed this effect to an important structural feature of the DiB NCs, that is, the existence of a potential barrier in the valence band at the core/shell interface created by a thin zinc-blende (ZB) CdS layer separating the ZB CdSe core from the wurtzite (WZ) region of the CdS shell (Figure 1a,b).[24] Together with electrostatic Coulomb repulsion, this barrier inhibits relaxation of the second hole into the core after it has captured the first hole. This phenomenon was referred to in ref 24 as "dynamic hole blockade".

Here we use this hole blocking mechanism to realize the regime of two-color electroluminescence (EL) from DiB NCs incorporated into LED structures. We demonstrate that the effective emission color of these DiB-LEDs can be tuned by varying an applied bias, which leads to changes in the relative intensities of core- and shell-related emission bands. To investigate the role of charge trapping on the emission efficiency and the branching between the core and the shell emission channels we conduct PL measurements on functional LEDs biased within the preinjection range. This approach allows us to modify the position of the Fermi level within the NCs and tune the occupancy of electron and hole trap states. Our results point to a dominant effect of shell-electron trapping on emission intensity and much lesser influence of core-charge trapping. This difference is attributed to a large dissimilarity in the spatial extent of wave functions of core- and shell-localized charges and a resulting difference in the strength of their coupling to nonradiative defect centers on the surface of the CdS shell.

Material Synthesis and Structural Characterization. To fabricate DiB NCs, we apply a modified version of a recently reported method for a quick growth of thick CdS shells developed for avoiding unintentional alloying at the CdSe/CdS interface.[25] This method allows for a highly reproducible synthesis of CdSe/CdS NCs with extremely thick shells that can be grown in a matter of a few hours with a small number of precursor injection steps (Figure 1c; see Methods for details). For example, using this method, the entire synthesis of the 20 nm CdSe/CdS NCs with a 7 nm thick shell is accomplished through only three injections over a total time of less than 6 h. This is considerably faster than the traditional synthetic protocol based on the successive ionic layer adsorption and reaction (SILAR),[14] which, for example, would require up to 40 steps performed consecutively over more than 50 h for growing a thinner 6 nm shell. Using the new method we can explore a much greater range of core radii and shell thicknesses than with the SILAR method, thereby achieving a wider range of color tunability. Importantly, we can also produce NCs with exceptionally thick CdS shells up to 9 nm, which is larger than the ∼3 nm Bohr exciton radius in CdS. In this size regime, the electronic structure of the core is quantized (the core radius R_0 = 1.5 nm is smaller than the exciton Bohr radius of CdSe ∼5.8 nm) while the shell can be described in bulklike terms. In conjunction with the quasi type-II band alignment at the interface,[18] this structure can be pictured as a bulklike colloidal particle with an engineered hole trap represented by the quantum-confined CdSe core (Figure 1b,c).[24]

Figure 1d shows transmission electron microscope (TEM) images of NCs with increasing shell thickness, H, and fixed radius R_0 = 1.5 nm. X-ray diffraction (XRD) patterns of the same NC samples are reported in Figure 1e together with XRD spectra of bulk CdSe and CdS for direct comparison. The XRD pattern of core-only NCs shows typical diffraction peaks of ZB CdSe. In agreement with previous observations for CdSe/CdS NCs, the first few monolayers of CdS grow epitaxially on top of the CdSe core (thin blue shell in Figure 1c).[26,27] Accordingly, the peaks sharpen and shift with increasing H to approach those of a bulk ZB CdS crystal, as expected due to increasing CdS domain size. Interestingly, when the shell thickness becomes larger than 3.5 nm, the crystal structure evolves to that of WZ CdS. As a result of this structural transition, DiB NCs have a shell primarily made of WZ CdS except for a fairly thin ZB layer directly adjacent to the CdSe core (Figure 1c). Coexistence of ZB and WZ CdS structural domains in the same NC has been recently observed by Mahler et al. for CdSe/CdS

dx.doi.org/10.1021/nl403478s | Nano Lett. 2014, 14, 486−494

NCs synthesized in the presence of primary amines.[28] The existence of a potential barrier at the heterointerface in CdSe/CdS dot-in-rod and tetrapods has also been recently invoked for explaining long residence times for both holes and electrons in the CdS region observed in single particle PL excitation experiments[10] and pulsed optically detected magnetic resonance measurements.[29]

Optical Properties of DiB Nanocrystals. In Figure 2, we show spectroscopic results for a set of CdSe/CdS NC samples

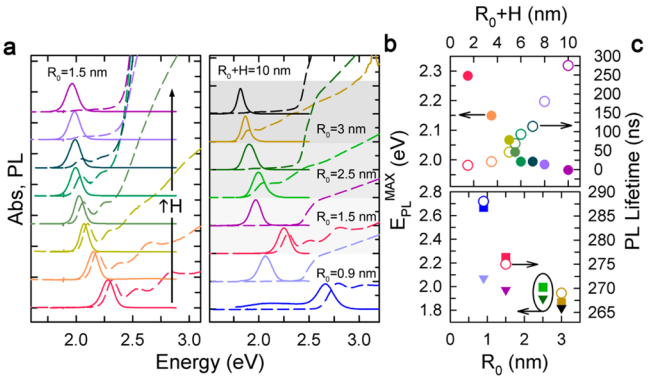

Figure 2. (a) Optical absorption (dashed lines) and PL spectra (solid lines) of core/shell CdSe/CdS NCs with core radius R_0 = 1.5 nm and increasing shell thickness (H = 0, 2, 3.5, 4, 4.5, 5.5, 6.5, and 8.5 nm). (b) Optical absorption (dashed lines) and PL (solid lines) spectra of core/shell CdSe/CdS NCs with a fixed total radius ($R_0 + H$ = 10 nm) and increasing core radius (R_0 = 0.9, 1.5, 2.5, and 3 nm) compared to similarly sized core-only NCs (samples with the same core size are grouped in gray shaded areas, the spectra of core-only CdSe NCs are the lower traces of each group). (c) Top panel: PL peak energy (solid circles) and PL lifetimes (open circles) for the same sample set as in panel a. Lower panel: PL peak energy (triangles) and PL lifetimes (open circles) for core/shell CdSe/CdS NCs with increasing core radius R_0 and the same total size $R_0 + H$ = 10 nm. The PL peak energy for corresponding core only CdSe NCs are shown by squares for direct comparisson to core/shell samples. The color scheme is the same throughout all panels.

with R_0 = 1.5 nm and increasing shell thickness (from H = 0 to 8.5 nm; Figure 2a) and for the NCs with a fixed total size ($R_0 + H$ = 10 nm) and increasing core radius (R_0 = 0.9 to 3 nm; Figure 2b). In Figure 2b, we report the absorption and PL spectra for the respective CdSe core particles for direct comparison with DiB NCs. Because of increasing leakage of the electron wave function into the shell region,[18,21] the PL spectrum of thicker shell NCs is progressively redshifted (Figure 2c, top panel; solid circles). Simultaneously, due to reducing electron–hole overlap, the PL lifetime (measured in the single-exciton regime; average NC excitonic occupancy $\langle N \rangle$ < 0.1) increases from ~10 ns for core-only CdSe NCs up to ~280 ns for the sample with the thickest shell (Figure 2c, top panel; open circles). NCs with increasing R_0 and same total size show a progressive red shift of the PL spectrum due to weaker quantum confinement of holes (Figure 2c, lower panel; solid triangles). In this case, electron–hole overlap arguments[21] predict shorter lifetimes for larger core NCs (larger electron–hole overlap), which is in agreement with our observations (Figure 2c, lower panel; open circles). Using CdSe/CdS NCs with various core and shell dimensions we achieve a wide-range spectral tunability of emitted light from 480 to 680 nm.

In Figure 3a, we show the pump-power dependent PL spectra of two representative samples of CdSe/CdS NCs of the

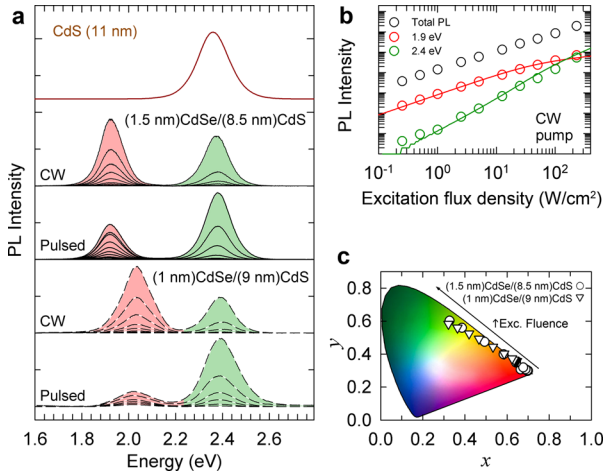

Figure 3. (a) PL spectra of CdSe/CdS DiB NCs with R_0 = 1.5 nm, H = 8.5 nm (solid lines) and R_0 = 1 nm, H = 9 nm (dashed lines) recorded using either cw or pulsed excitation with a progressivly increasing fluence. These spectra show simultaneous emission from the CdSe core (red shading) and the thick CdS shell (green shading). The PL spectrum of 20 nm core-only CdS NCs is included for comparison (brown line at the top). (b) The intensities of core (red circles) and shell (green circles) emission for CdSe/CdS NCs (R_0 = 1.5 nm, H = 8.5 nm) as a function of cw excitation fluence plotted on a log–log scale. The total PL intensity (black circles) has been multiplied by a factor of 10 for clarity. Evolutions of the two emission features simulated using a core-blocking model (see ref 24) are shown by solid lines. (c) Pump-intensity dependent emission from the DiB NCs projected onto the CIE (Commission Internationale de l'Éclairage) chromaticity diagram based on PL spectra shown in panel a.

same overall size (10 nm radius) but different core radii, 1.5 nm (solid lines) and 1 nm (dashed lines). Using 3.1 eV excitation, which is above the energy gap of both CdSe and CdS, we generate electron-hole pairs primarily in the shell (which has a much greater absorption cross-section than the core[18]). At a low fluence, the PL spectrum of both samples shows a single peak (at 1.9 and 2.05 eV for R_0 = 1.5 nm and R_0 = 1 nm, respectively) due to radiative recombination of a delocalized electron with a core-localized hole ("core emission"). As the excitation fluence is increased, we observe the emergence of a higher energy PL band at 2.4 eV, which first grows linearly, then superlinearly and finally linearly again. Similar trends are also observed under pulsed excitation (see Supporting Information Figure S1). This emission energy is near the band gap of bulk CdS and is therefore ascribed to electron–hole recombination in the CdS shell ("shell emission"). Remarkably, while the core emission shows saturation with increasing fluence (red circles in Figure 3b), the shell emission keeps growing (green circles) and so does the total PL intensity (black circles), suggesting that the overall PL quantum yield does not appreciably drop at high excitation fluence. In a recent study, we investigated this behavior in detail via single-particle spectroscopy, which pointed to a Coulomb blockade mechanism that prevents the localization of a second hole in the core when it is already occupied by a hole.[24] This effect prevents the formation of multiexcitons in the core region and consequent activation of Auger recombination[24] which would otherwise cause saturation of the spectrally integrated (total) PL intensity at high pump intensities, typical exhibited by conventional NCs. Using this pump-power-controlled branch-

dx.doi.org/10.1021/nl403478s | Nano Lett. 2014, 14, 486–494

ing between the core- and shell-related emission channels we can continuously tune the effective emission color of the DiB NCs from red to green, as illustrated by the color trajectory in Figure 3c.

DiB NC-Based Devices: Color Tunable LEDs with Dual Emission. The peculiar photophysics of DiB NCs allows for achieving an interesting regime of dual-emission under electrical excitation. In previous studies on LEDs based on CdSe/CdS hetero-NCs, including "giant" quantum dots,[30] EL from shell states was not observed because of very fast relaxation of injected holes into core states. Optical pumping of conventional CdSe/CdS structures does allow for observation of shell emission, however it requires excitation with intense, ultrashort pulses (e.g., 100 fs), which is necessary for achieving high exciton generation rates exceeding that of nonradiative Auger recombination.[18,22]

The phenomenon of dynamic hole blockade[24] allows one to circumvent these limitations. Specifically, because of this effect the core hole occupancy in these NCs never exceeds one, preventing the activation of fast Auger decay. As a result, DiB NCs exhibit two-color EL at fairly low current densities of a few tenths of A/cm^2. In Figure 4a, we report EL spectra of LEDs comprising a thin film of DiB NCs (1−2 monolayers) with two different core and shell sizes: R_0 = 1.5 nm and H = 8.5 nm (solid red curves) and R_0 = 1 nm and H = 9 nm (dashed blue curves). The emitting DiB NC layer is sandwiched between a poly(3,4-ethylenedioxythiophene):poly(styrenesulfonate) (PEDOT:PSS) hole-injecting layer spin-coated onto a patterned indium tin oxide (ITO) substrate and a thermo-evaporated LiF(2 nm)/Al(100 nm) cathode (Figure 4a, top right panel). The EL spectra exhibit both core and shell emission bands immediately at the turn-on voltage ($V_{ON} \approx$ 8 and 4 V for devices with R_0 = 1.5 and 1 nm, respectively). As the voltage is increased, the shell EL grows faster than core emission (lower right panel of Figure 4a), which results in an overall yellow color at V > 6 V (see the photographs in the inset of Figure 4b; the respective Commission Internationale de l'Éclairage, CIE, chromaticity coordinates are shown in Supporting Information Figure S2). This behavior is in agreement with the pump-intensity dependent PL data in Figure 3 and is again derived from the phenomenon of dynamic core blockade.[24] Without this effect, excitation of the shell emission would require much higher current densities that are not likely realizable in these fairly resistive structures.[31]

Despite their simple architecture, these proof-of-principle dual-color LEDs show good performance. Their emission is highly spatially uniform (inset of Figure 4b), and the efficiency and the brightness are as high as 0.1% and 2000 cd/m^2, respectively (Figure 4b). The devices were tested in air without additional environmental protection and did not exhibit any degradation in EL for several days. The observed external quantum efficiency (EQE) is over 2 orders of magnitude higher than that of single-color NC-based devices of similar architecture (~6 × 10^{-3} cd/A for CdSe/ZnS NCs based LEDs)[32] and is comparable to that of LEDs made of CdSe/CdS g-NCs synthesized through a conventional SILAR method.[30] Importantly, these latter devices showed EL exclusively in the red (core emission) without any signs of shell emission in the green despite the apparent similarity of g-NCs with our DiB structures.

We note that these proof-of-principle devices have not been optimized in terms of the active layer thickness or electrodes work functions and therefore do not allow for balanced

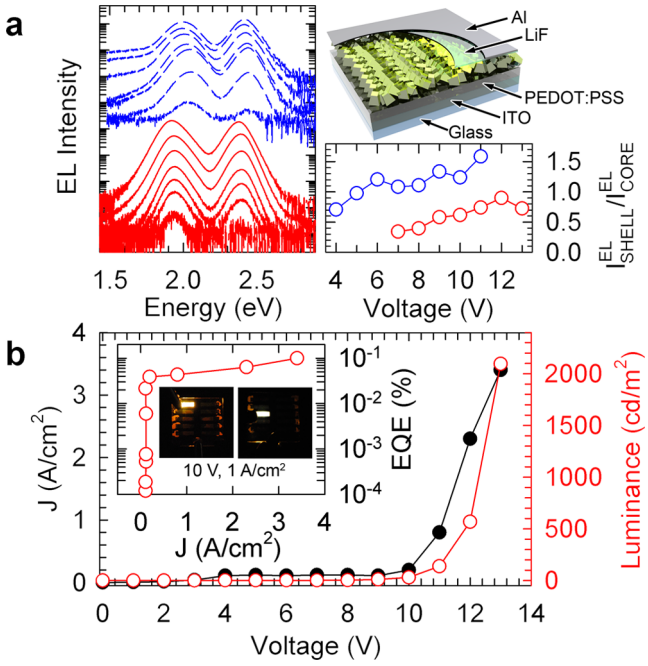

Figure 4. (a) Left panel: Dual-color EL from two different DiB NC LEDs (R_0 = 1.5 nm, H = 8.5 nm, red curves; R_0 = 1 nm, H = 9 nm, blue curves, semilogarithmic scale) for a progressively increasing bias (V). The respective CIE chromaticity coordinates are shown in Supporting Information Figure S2. Top panel on the right: Schematics of the device comprising 1 to 2 monolayers of CdSe/CdS DiB NCs sandwiched between a PEDOT:PSS (100 nm) coated ITO anode and a LiF(2 nm)/Al(100 nm) cathode. Bottom panel on the right: The ratio of intensities of the shell (2.4 eV for both NC samples) and core emission (1.9 eV for NCs with R_0 = 1.5 nm, red circles; and 2.05 eV for NCs with R_0 = 1 nm, blue circles) as a function of V; the relative contribution of the green component progressively increases with increasing driving voltage. (b) Current density (J; black circles) and luminance (red open circles) versus applied voltage for the NC-LED made of CdSe/CdS NCs with R_0 = 1.5 nm and H = 8.5 nm. Inset: external quantum efficiency (EQE) for emission from the top face of the device as a function of current density j. The inset also shows photographs of functioning LEDs (left, R_0 = 1.5 nm, H = 8.5 nm; right, R_0 = 1 nm, H = 9 nm) biased with 10 V (J = 1 A/cm^2).

injections of electrons and holes, which is one of the primary factors limiting the device EQE. An improved performance can potentially be achieved by adopting, for example, an inverted device architecture in which the ITO substrate coated with ZnO nanoparticles serves as a cathode while a hole-conducting organic layer capped with molybdenum oxide and aluminum serves as an anode.[33] Using this LED design efficiencies as high as 18% in the red,[34] 6% in the green, and 1.7% in the blue have recently been obtained.[35] This more advanced architecture can potentially also suppress "unwanted" electronic coupling between the NCs and the electrodes, which significantly affects the emission efficiency in our presently used structures (see next section).

Electrical Control of Two-Color Emission. To better understand the behavior of our DiB NC-LEDs, we performed PL measurements on devices under an applied bias in a range of voltages below the EL turn-on threshold. Functional LEDs as well as control devices (see below) were excited with a cw laser at 3.1 eV (excitation flux density 75W/cm^2) through the transparent ITO/PEDOT:PSS anode and the emission was collected in backscattering geometry through a dichroic filter.

dx.doi.org/10.1021/nl403478s | Nano Lett. 2014, 14, 486−494

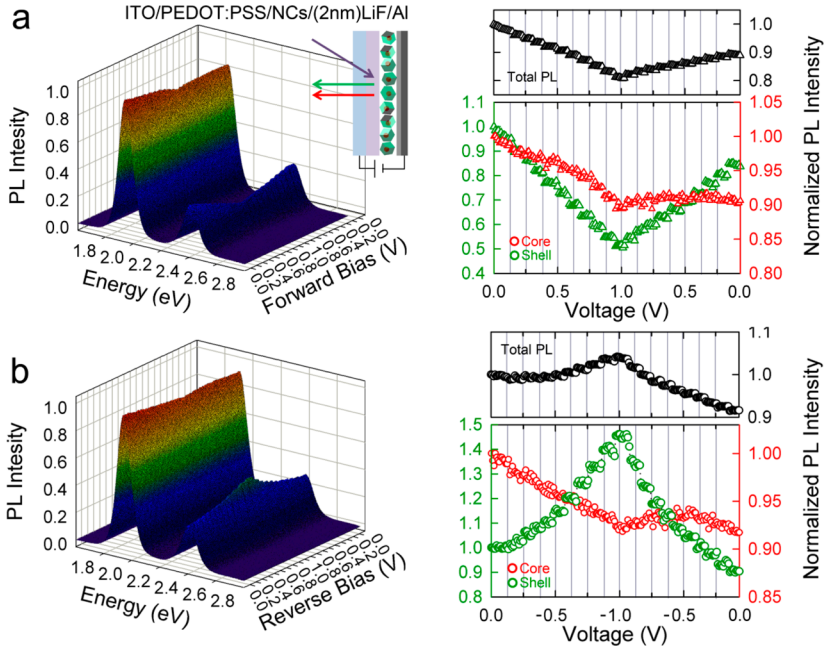

Figure 5. (a) Left panel: Series of PL spectra (0.5 s acquisition/frame; excitation at 3.1 eV) of a thin film (1−2 monolayer thickness) of DiB NCs (R_0 = 1.5 nm, H = 8.5 nm) during a stepwise voltage scan in forward bias. Inset: Schematics of the device comprising 1 monolayer of CdSe/CdS DiB NCs sandwiched between a PEDOT:PSS(100 nm)-coated ITO anode and a LiF(2 nm)/Al(100 nm) cathode. Right panel: PL intensity extracted from the PL spectra for both core (red symbols) and shell (green symbols) emission under forward bias. The total integrated PL intensity is reported in open circles. (b) Series of PL spectra (0.5 s acquisition/frame; excitation at 3.1 eV) of the same device as in panel a during a stepwise voltage scan in reverse bias. The PL intensity for core and shell emission as well as the total PL intensity is shown in the right panel.

Figure 5 reports the evolution of PL spectra and the core and shell emission intensities for DiB NC-LEDs for stepwise voltage ramps for both forward (Figure 5a) and reverse (Figure 5b) biases. The total PL intensity is also shown for both polarities. Application of a forward bias (positive potential on the ITO/PEDOT:PSS anode and negative on the metal cathode) quenches both core and shell emission, which results in the decrease of the overall PL intensity. The two bands show opposite trends under reverse bias. Specifically, as the reverse bias is increased to −1 V, the shell PL intensity is increased by ∼50%, while core emission is slightly decreased (by ∼5%). As a result of these changes, the overall emission yield is increased.

The observed bias-induced changes in PL can be either due to applied electric field[36,37] and/or direct electronic communication (that is, exchange of charges) between the NCs and the electrodes (see an approximate energy diagram of the device in Figure 6a). To test the role of electric field and to decouple the effects of NC interactions with a cathode versus an anode, we have fabricated control devices with additional interlayers that selectively isolate the electrodes from the NC active layer. Specifically, we investigated the following control structures: **A**, ITO/PEDOT:PSS/PVK/NCs/(2 nm)LiF/Al, incorporating an additional polyvinyl carbazole (PVK) electron blocking layer (100 nm) isolating the NC active layer from the PEDOT:PSS electrode; **B**, ITO/PEDOT:PSS/NCs/(40 nm)-LiF/Al, featuring a thick dielectric LiF interlayer, which isolates the Al cathode from the NCs; and **C**, ITO/PEDOT:PSS/(40 nm)LiF/NCs/(40 nm)LiF/Al where both electrodes are isolated from the NC emitting layer. An approximate energy diagram of the control devices is shown in the top panel of Figure 6b.

In control device **A**, the PVK layer suppresses electron transfer between the dots and the PEDOT:PSS anode as PVK's lowest unoccupied molecular orbital (LUMO) level (2.2 eV) is much higher than the conduction band edges of either CdSe (4.0 eV) or CdS (3.85 eV). On the other hand, a 1−2 nm thick LiF interlayer introduces a tunneling barrier, which prevents quenching of the NC chromophores by the metal cathode while still allowing for electron transfer from the metal to the NCs. In contrast to this partial isolation of the NCs from the cathode, a 40 nm thick LiF film completely blocks charge transfer to/from the electrodes in control devices **B** and **C**. To summarize this description of reference structures, in control device **A** the dots can only exchange electrons with the metal cathode; in control device **B**, the properties of the NC active layer are determined exclusively by its interactions with the anode; and finally, in control device **C**, the NCs are isolated from both electrodes and can only be affected by the applied electric field.

The PL from control devices **A** and **C** shows a distinctly different behavior compared to that of functional LEDs (Figure 6b). Specifically, the PL intensity for both core and shell bands remains unchanged for either direction of the applied bias. This suggests, first, that it is not the electric field that is responsible for the observed changes in PL and, second, that in the range of preinjection voltages used in these measurements there is no charge transfer between the metal cathode and the NCs.

Next, we study reference structure **B**, in which the NC active layer is electrically isolated from the metal cathode but is in direct contact with the ITO/PEDOT:PSS anode. This structure exhibits exactly the same bias-dependent changes in PL as a functional LED (compare Figure 6b to Figure 5a,b). This indicates that the observed trends are due to direct exchange of charges between the anode and the NCs, as also confirmed by measurements of PL dynamics (see Figure S4 of Supporting Information). This further suggests that the anode and the NC emitting layer can be described by a common Fermi level, and hence, the applied bias influences NC emission through the

dx.doi.org/10.1021/nl403478s | Nano Lett. 2014, 14, 486−494

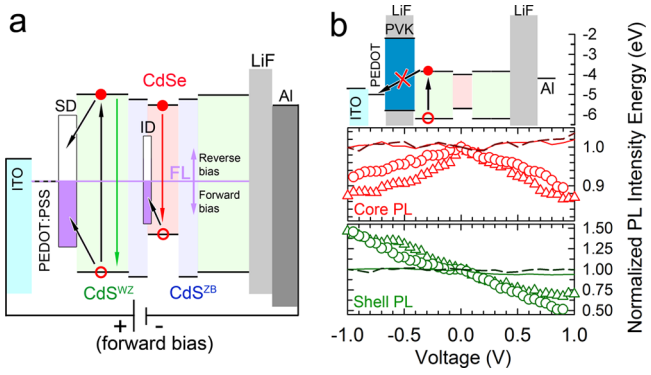

Figure 6. (a) Energy level diagram of a ITO/PEDOT:PSS/DiB CdSe-CdS NCs/LiF/Al junction. The LiF interlayer (shaded in gray) introduces a dielectric barrier that partially isolates the Al cathode. The position of the Fermi Level (FL, purple line) is determined by the ITO/PEDOT:PSS substrate that is in direct contact with the NCs and defines the occupancy of surface and interfacial intragap defect states (denoted as SD and ID, respectively). For simplicity, it is assumed that electrons and shell-localized holes are affected primarily by SD states, while core-localized holes by ID states. Application of a forward (reverse) bias lowers (raises) the anode FL and thereby activates (passivates) electron traps; the applied bias has an opposite effect on hole traps. (b) Top panel: An approximate energy level diagram of control devices incorporating additional blocking layers to selectively isolate the electrodes from the NC active layer: control device **A** incorporates a 100 nm thick polyvinyl carbazole (PVK) blocking layer (blue shading) at the PEDOT:PSS/DiB-NC interface; control device **B** features a thick (40 nm) LiF electron-blocking layer at the DiB-NC/Al interface (gray shading); and **C** incorporates thick (40 nm) LiF layers on both sides of the NC active layer (gray shading), electrically isolating both electrodes from the DiB-NCs. Comparison of the PL response under applied bias (core PL, central panel, shell PL lower panel) of a functional LED shown in Figure 5 (circles) and the control devices: **A** (solid red line), **B** (triangles), and **C** (dashed black line).

change in the position of the Fermi level with regard to NC conduction and valence band edge, as in the case of spectro-electrochemical experiments[38] or in a traditional metal-insulator-semiconductor structure formed by an Al layer (metal gate electrode), LiF insulator, and a layer of semiconductor NCs.

As shown by previous spectro-electrochemical studies,[38−43] by raising (lowering) the Fermi level one can achieve direct injection of electrons (holes) into NC band edge states. The injection of carriers into the band edge states modifies the PL due to changes in the emission rate as well as the activation of nonradiative Auger decay.[38,44] In principle, even though in our PL measurements we investigate the range of subthreshold voltages, one type of carriers (electrons or holes) can still be injected into the conduction- or valence-band states of the NCs without activating EL. The effect of NC charging due to interactions with electrodes was recently observed in "inverted" NC-LEDs with a cathode made of ITO coated with ZnO nanoparticles.[33,45] Because of the fairly high Fermi level of the ZnO layer, electrons were spontaneously injected into the conduction band-edge state even under zero bias as was indicated by PL dynamics, which exhibited typical signatures of charged exciton Auger recombination. In our structures with an ITO/PEDOT:PSS anode, the Fermi level of the electrode is lower than that of ZnO nanoparticles, therefore, the likelihood of electron injection into the band-edge state is reduced.

To test the possibility of electron transfer from the ITO/PEDOT:PSS electrode to NC quantized level in our LED structures, we have performed time-resolved PL measurements under an applied bias. As shown in previous works,[38,41,44,46] direct injection of charges into NC band-edge states leads to the formation of positive (in the case of injection of holes) or negative (due to injection of electrons) trions. This results in the increase of the initial PL intensity at zero delay due to doubling of the radiative rate and faster PL relaxation due to both the accelerated radiative decay and activation of nonradiative Auger recombination. The PL dynamics measured for our LEDs (see Supporting Information Figure S3) show behavior that is inconsistent with the formation of trions. Specifically, we observe that under reverse bias the initial PL intensity is indeed increased. However, instead of the accelerated PL decay, expected for trions, the PL lifetime becomes longer. Similarly, application of forward bias leads to the reduction of the initial PL intensity and shortening of the PL lifetime, which is again inconsistent with the formation of trions. These results show that in our measurements the variation in the Fermi level induced by applied bias is not sufficiently large to inject charges into the NC band edge states. Instead, the Fermi level is tuned within the intragap region. However, as was demonstrated in refs 39 and 40, even in this case it can still affect PL due to changes in the occupancy of NC intragap defect states, which modifies the rate of defect-related nonradiative losses. As we show below, this effect allows for a consistent explanation of the bias-dependent PL changes observed in our measurements.

In the phenomenological model proposed in ref 40, electron and hole traps are assumed to form two semicontinuous intragap bands whose filling is defined by the position of the Fermi level. For electron traps, raising the Fermi energy leads to a progressive filling of the trap states, reducing the number of available trapping sites, thereby suppressing defect-mediated electron relaxation.[36] Hole traps are expected to follow the opposite trend, where lowering the Fermi energy removes carriers from the traps. This increases the available trap density, which results in enhanced defect-related hole relaxation.[36] In the case of DiB NCs, modifications of the electron and hole trapping are expected to have different effects on the core vs shell emission. As was shown previously,[24] the dynamics of holes residing in the DiB NC shell is dominated by very fast capture (ca. 10−20 ps) by core states, which outpaces trapping at defect sites. As a result, the bias-induced shift of the Fermi level is expected to affect the shell emission primarily through the electron-trapping channel. Specifically, increased reverse bias, which raises the Fermi level, should lead to increasing filling of electron traps and hence enhanced shell emission because of the suppression of defect-related electron relaxation. This reasoning is indeed consistent with the experimentally observed increase in the shell emission efficiency under reverse bias (Figure 5b).

A slight reduction in the core emission efficiency observed under the same conditions is likely due to increasing number of trap sites that become available for core-localized holes in the case of the raising Fermi level. The core holes are much longer lived than holes residing in the NC shell and therefore are more strongly affected by the defect-related relaxation channel. A significantly smaller effect of reverse bias on core emission than on shell emission is likely because the increase in the number of hole traps is partially compensated by the decrease in the rate of defect-related electron relaxation due to filling of electron trap sites, as discussed above. PL measurements under direct excitation of the core at 2.29 eV (that is, below the absorption

dx.doi.org/10.1021/nl403478s | Nano Lett. 2014, 14, 486−494

onset of the CdS shell) show a similar trend for the core emission (Supporting Information Figure S5). Specifically, we observe a progressive reduction in the core PL intensity under increasing reverse bias, which can again be attributed to the activation of intragap hole trap sites. This result further suggests that the hole traps are likely associated with structural defects at the core/shell interface (labeled ID in Figure 6a).

Similar considerations can be applied to explain changes in PL under forward bias, which corresponds to lowering the Fermi energy. In this situation, the increasing availability of electron trap sites accelerates defect-related electron relaxation, which should diminish the intensities of both shell and core emission since both involve the same electron state delocalized over the entire NC. A simultaneous decrease in the number of available hole trap sites is likely unable to reverse this trend, as hole trapping has only a little effect on shell emission (see our earlier discussion) while in the case of core-localized holes it is likely outpaced by electron trapping (core-localized holes are better isolated from traps on the surface of a CdS shell than delocalized electrons). The fact that a fairly large change in the core emission under direct bias is dominated by changes in the electron trapping channel seems to contradict our earlier assessment that for the reverse bias the change in the core PL is defined by changes in the hole trapping channel which slightly outcompetes the opposite trend due to electron trapping. A similar situation, however, has been realized and quantitatively modeled in previous spectro-electrochemical studies of dual emission from Cu-doped NCs.[40] As was proposed in this reference, the asymmetry in response to direct versus reverse bias likely arises from the difference in spectral distributions of electron and hole intragap states and the difference in capture cross sections for the two types of carriers.

Interestingly, in the case of direct excitation of the core (2.29 eV pump) application of forward bias does not lead to considerable changes in the core emission intensity (Supporting Information Figure S5) in contrast to the reduction in the core-related PL signal for the situation of shell excitation (3.1 eV pump). This might suggest that the exact nature of photoexcited electron states is different between the two cases. Specifically, as was suggested in ref 47, the presence of a hole in the CdSe core leads to the localization of the electron within the attractive Coulomb potential of the positively charged core region. In the case of 3.1 eV excitation, the formation of this Coulombically bound state is delayed with regard to the initial photon absorption event by, first, the time of hole trapping into the core and then, electron localization within the hole Coulomb potential. As a result, the electron has a more prolonged time for interacting with traps on the surface of the CdS shell compared to the situation of direct excitation of the core when a core-bound exciton is created immediately following absorption of a photon. Consequently, the effect of "depassivation" of surface electron traps due to lowering the Fermi level is less pronounced in the case of the lower energy 2.29 eV excitation compared to excitation at 3.1 eV.

Conclusions. We have studied light-emitting properties of recently introduced DiB NCs that comprise quantum-confined CdSe cores overcoated with extremely thick bulk-like CdS shells. These nanostructures feature two interdependent emission channels and allow for facile manipulation of the effective emission color by varying the excitation power. In addition to dual emission achievable even under weak cw optical excitation, they show efficient two-color EL. The unusual properties of DiB NCs are derived from the unique internal structure that features a thin hole-blocking barrier at the core−shell interface. This barrier facilitates the development of a core-blocking mechanism, which limits the core hole occupancy to one and allows for the development of shell emission at low excitation rates corresponding to the slow radiative recombination of a core hole with delocalized electrons. This is in contrast to previously reported CdSe/CdS heterostructures in which the CdSe core can be occupied with multiple holes and hence the saturation of core states requires extremely high pumping rates to outpace the rate of nonradiative Auger recombination.[48] In this latter case, shell emission cannot be observed under either cw optical or electrical pumping but instead requires excitation with high intensity, ultrashort laser pulses. Finally, we performed PL measurements on functional DiB-NC-LEDs and investigate the effects of applied electrical bias on their emission properties. Using electron/hole blocking layers to selectively isolate the electrodes from the active NC layer, we demonstrate that the bias-induced modulation of core and shell emission is not due to the applied electric field but instead results from charge transfer between the anode and intragap states likely residing on the NC surfaces. These measurements also suggest that the main factor limiting emission efficiency in these NCs is trapping of electrons at intragap states while the process of nonradiative hole trapping is less significant.

Methods. *Synthesis.* Zinc blende CdSe NCs were synthesized by previously reported methods.[49] For the synthesis of CdSe (R_0 = 1.5 nm)/CdS NCs, 2 × 10^{-7} mol of CdSe NCs (purified twice) dispersed in 10 mL of 1-octadecene (ODE) was loaded in a 100 mL flask, degassed at 110 °C for 1 h, filled with Ar, and heated up to 300 °C for CdS shell growth. A 0.2 mmol sample of Cd-oleate and 0.2 mmol of 1-dodecanethiol were added slowly (0.1 mmol/min) and the reaction was maintained at the elevated temperature for 30 min to form thin CdS buffer layers (~3 monolayers) on top of CdSe cores. For further CdS shell growth, a mixed solution of Cd-oleate and trioctylphospine-sulfur (0.5 M/0.5M) in ODE was continuously added at a rate of 1 mmol/hour at 300 °C. After the injection of precursors was completed, the reaction products were cooled to room temperature and purified repeatedly by a precipitation-and-redispersion method. The final products were dispersed in hexane for further characterization.

Spectroscopic Studies. Spectroscopic measurements reported in Figures 2 and 3 and Supporting Information Figure S1 were carried out using hexane solutions of NCs loaded into quartz cuvettes. In the measurements of PL dynamics, the samples were vigorously stirred to avoid the effects of photocharging.[50] Absorption spectra of NC solutions were measured with an Agilent 8543 UV−vis spectrophotometer. Steady state PL measurements were performed by exciting samples at 3.1 eV with a cw Coherent Cube laser and collecting spectrally resolved emitted light with a charged coupled device. Transient PL measurements were carried out using <70 ps pulses at 3.1 eV from a pulsed diode laser (Picoquant LDH-P series). The emitted light was collected with a multichannel plate detector coupled to time-correlated single-photon counting electronics (time resolution ~100 ps). Higher temporal resolution studies of shell emission dynamics shown in Supporting Information Figure S2a (lower panel) were performed using a streak camera (time resolution ~12 ps); in these measurements, the samples were excited at 3.1 eV using

dx.doi.org/10.1021/nl403478s | Nano Lett. 2014, 14, 486−494

frequency-doubled 250 fs pulses from an amplified 1 kHz Ti:Sapphire laser.

Fabrication and Characterization of NC LEDs. LED structures comprise a DiB NC active layer (1 to 2 NC monolayers) sandwiched between a poly(3,4-ethylendioxythiophene):poly(styrenesulfonate) (PEDOT:PSS) coated indium tin oxide (ITO) anode and a LiF/Al cathode; ITO-coated glass substrates were cleaned in isopropanol prior to use. The PEDOT:PSS layer (100 nm) was spin coated onto the substrate and annealed at 250 °C for 20 min inside an inert atmosphere (ultra high purity Ar) glovebox. The high-temperature annealing yields a compact hole-conducting layer. The DiB NC active layer was then spin coated (2500 rpm) from a 10 mg/mL NC octane solution. Finally, 2 nm of LiF and 100 nm of aluminum were thermally evaporated onto the NC layer through a shadow mask to form the top electrode. A Keithley 2400 source meter was used to measure the current−voltage characteristics of the devices. The light output was measured by a calibrated Newport power meter (model 1830) with a Newport silicon photodetector positioned at a fixed distance and directed toward the ITO glass side of the device. The LED brightness was determined from the fraction of light that reaches the photodetector. The EL spectra were recorded with a spectrometer (Ocean Optics, Inc.) coupled to an optical fiber. NC-LEDs were tested in air without additional environmental protection. The devices were stored under ambient conditions between experiments.

■ ASSOCIATED CONTENT

Supporting Information

Additional results of spectroscopic and electroluminescence characterization of DiB CdSe/CdS NCs. This material is available free of charge via the Internet at http://pubs.acs.org.

■ AUTHOR INFORMATION

Corresponding Authors

*E-mail: (V.I.K.) klimov@lanl.gov.

*E-mail: (S.B.) sergio.brovelli@unimib.it.

Notes

The authors declare no competing financial interest.

■ ACKNOWLEDGMENTS

W.K.B and V.I.K. are supported by the Chemical Sciences, Biosciences, and Geosciences Division of Office of Science, Office of Basic Energy Sciences (BES), U.S. Department of Energy (DOE). S.B., F.M., and U.G. acknowledge support from Cariplo Foundation (Grant N.2012-0844). S.B. wishes to thank the European Community's Seventh Framework Programme (FP7/2007-2013) under Grant N. 324603.

■ REFERENCES

(1) Bae, W. K.; Kwak, J.; Lim, J.; Lee, D.; Nam, M. K.; Char, K.; Lee, C.; Lee, S. Multicolored Light-Emitting Diodes Based on All-Quantum-Dot Multilayer Films Using Layer-by-Layer Assembly Method. *Nano Lett.* **2010**, *10* (7), 2368.

(2) Dang, C.; Lee, J.; Breen, C.; Steckel, J. S.; Coe-Sullivan, S.; Nurmikko, A. Red, green and blue lasing enabled by single-exciton gain in colloidal quantum dot films. *Nat. Nanotechnol.* **2012**, *7* (5), 335.

(3) Klimov, V. I.; Mikhailovsky, A. A.; Xu, S.; Malko, A.; Hollingsworth, J. A.; Leatherdale, C. A.; Eisler, H. J.; Bawendi, M. G. Optical gain and stimulated emission in nanocrystal quantum dots. *Science* **2000**, *290* (5490), 314.

(4) Alivisatos, A. P.; Gu, W. W.; Larabell, C. Quantum dots as cellular probes. *Annu. Rev. Biomed. Eng.* **2005**, *7*, 55.

(5) Dubertret, B.; Skourides, P.; Norris, D. J.; Noireaux, V.; Brivanlou, A. H.; Libchaber, A. In Vivo Imaging of Quantum Dots Encapsulated in Phospholipid Micelles. *Science* **2002**, *298* (5599), 1759.

(6) Otto, T.; Müller, M.; Mundra, P.; Lesnyak, V.; Demir, H. V.; Gaponik, N.; Eychmüller, A. Colloidal Nanocrystals Embedded in Macrocrystals: Robustness, Photostability, and Color Purity. *Nano Lett.* **2012**, *12* (10), 5348.

(7) Brokmann, X.; Messin, G.; Desbiolles, P.; Giacobino, E.; Dahan, M.; Hermier, J. P. Colloidal CdSe/ZnS quantum dots as single-photon sources. *New. J. Phys.* **2004**, *6* (1), 99.

(8) Klimov, V. I. *Nanocrystal Quantum Dots*, Second ed.; Taylor and Francis: New York, 2009.

(9) Donega, C. d. M. Synthesis and properties of colloidal heteronanocrystals. *Chem. Soc. Rev.* **2011**, *40* (3), 1512.

(10) Borys, N. J.; Walter, M. J.; Huang, J.; Talapin, D. V.; Lupton, J. M. The Role of Particle Morphology in Interfacial Energy Transfer in CdSe/CdS Heterostructure Nanocrystals. *Science* **2010**, *330* (6009), 1371.

(11) Rainó, G.; Stöferle, T.; Moreels, I.; Gomes, R.; Kamal, J. S.; Hens, Z.; Mahrt, R. F. Probing the Wave Function Delocalization in CdSe/CdS Dot-in-Rod Nanocrystals by Time- and Temperature-Resolved Spectroscopy. *ACS Nano* **2011**, *5* (5), 4031.

(12) Cassette, E.; Mahler, B.; Guigner, J.-M.; Patriarche, G.; Dubertret, B.; Pons, T. Colloidal CdSe/CdS Dot-in-Plate Nanocrystals with 2D-Polarized Emission. *ACS Nano* **2012**, *6* (8), 6741.

(13) Mahler, B.; Spinicelli, P.; Buil, S.; Quelin, X.; Hermier, J.-P.; Dubertret, B. Towards non-blinking colloidal quantum dots. *Nat. Mater.* **2008**, *7* (8), 659.

(14) Chen, Y.; Vela, J.; Htoon, H.; Casson, J. L.; Werder, D. J.; Bussian, D. A.; Klimov, V. I.; Hollingsworth, J. A. "Giant" Multishell CdSe Nanocrystal Quantum Dots with Suppressed Blinking. *J. Am. Chem. Soc.* **2008**, *130* (15), 5026.

(15) Spinicelli, P.; Buil, S.; Quélin, X.; Mahler, B.; Dubertret, B.; Hermier, J. P. Bright and Grey States in CdSe-CdS Nanocrystals Exhibiting Strongly Reduced Blinking. *Phys. Rev. Lett.* **2009**, *102* (13), 136801.

(16) Chen, O.; Zhao, J.; Chauhan, V. P.; Cui, J.; Wong, C.; Harris, D. K.; Wei, H.; Han, H.-S.; Fukumura, D.; Jain, R. K.; Bawendi, M. G. Compact high-quality CdSe−CdS core−shell nanocrystals with narrow emission linewidths and suppressed blinking. *Nat. Mater.* **2013**.

(17) García-Santamaría, F.; Brovelli, S.; Viswanatha, R.; Hollingsworth, J. A.; Htoon, H.; Crooker, S. A.; Klimov, V. I. Breakdown of Volume Scaling in Auger Recombination in CdSe/CdS Heteronanocrystals: The Role of the Core−Shell Interface. *Nano Lett.* **2011**, *11* (2), 687.

(18) García-Santamaría, F.; Chen, Y. F.; Vela, J.; Schaller, R. D.; Hollingsworth, J. A.; Klimov, V. I. Suppressed Auger Recombination in "Giant" Nanocrystals Boosts Optical Gain Performance. *Nano Lett.* **2009**, *9* (10), 3482.

(19) Zavelani-Rossi, M.; Lupo, M. G.; Tassone, F.; Manna, L.; Lanzani, G. Suppression of Biexciton Auger Recombination in CdSe/CdS Dot/Rods: Role of the Electronic Structure in the Carrier Dynamics. *Nano Lett.* **2010**, *10* (8), 3142.

(20) Javaux, C.; Mahler, B.; Dubertret, B.; Shabaev, A.; Rodina, A. V.; Efros, A. L.; Yakovlev, D. R.; Liu, F.; Bayer, M.; Camps, G.; Biadala, L.; Buil, S.; Quelin, X.; Hermier, J.-P. Thermal activation of non-radiative Auger recombination in charged colloidal nanocrystals. *Nat. Nanotechnol.* **2013**, *8*, (3).

(21) Brovelli, S.; Schaller, R. D.; Crooker, S. A.; García-Santamaría, F.; Chen, Y.; Viswanatha, R.; Hollingsworth, J. A.; Htoon, H.; Klimov, V. I. Nano-engineered electron-hole exchange interaction controls exciton dynamics in core-shell semiconductor nanocrystals. *Nat. Commun.* **2011**, 2.

(22) Krahne, R.; Zavelani-Rossi, M.; Lupo, M. G.; Manna, L.; Lanzani, G. Amplified spontaneous emission from core and shell

transitions in CdSe/CdS nanorods fabricated by seeded growth. *Appl. Phys. Lett.* **2011**, *98* (6), 063105.
(23) Lutich, A. A.; Mauser, C.; Da Como, E.; Huang, J.; Vaneski, A.; Talapin, D. V.; Rogach, A. L.; Feldmann, J. Multiexcitonic Dual Emission in CdSe/CdS Tetrapods and Nanorods. *Nano Lett.* **2010**, *10* (11), 4646.
(24) Galland, C.; Brovelli, S.; Bae, W. K.; Padilha, L. A.; Meinardi, F.; Klimov, V. I. Dynamic Hole Blockade Yields Two-Color Quantum and Classical Light from Dot-in-Bulk Nanocrystals. *Nano Lett.* **2012**, *13* (1), 321.
(25) Bae, W. K.; Padilha, L. A.; Park, Y.-S.; McDaniel, H.; Robel, I.; Pietryga, J. M.; Klimov, V. I. Controlled Alloying of the Core−Shell Interface in CdSe/CdS Quantum Dots for Suppression of Auger Recombination. *ACS Nano* **2013**, *7* (4), 3411.
(26) Lim, S. J.; Chon, B.; Joo, T.; Shin, S. K. Synthesis and Characterization of Zinc-Blende CdSe-Based Core/Shell Nanocrystals and Their Luminescence in Water. *J. Phys. Chem. B* **2008**, *112* (6), 1744.
(27) Peng, X.; Schlamp, M. C.; Kadavanich, A. V.; Alivisatos, A. P. Epitaxial Growth of Highly Luminescent CdSe/CdS Core/Shell Nanocrystals with Photostability and Electronic Accessibility. *J. Am. Chem. Soc.* **1997**, *119* (30), 7019.
(28) Mahler, B.; Lequeux, N.; Dubertret, B. Ligand-Controlled Polytypism of Thick-Shell CdSe/CdS Nanocrystals. *J. Am. Chem. Soc.* **2009**, *132* (3), 953.
(29) van Schooten, K. J.; Huang, J.; Baker, W. J.; Talapin, D. V.; Boehme, C.; Lupton, J. M. Spin-Dependent Exciton Quenching and Spin Coherence in CdSe/CdS Nanocrystals. *Nano Lett.* **2012**, *13* (1), 65.
(30) Pal, B. N.; Ghosh, Y.; Brovelli, S.; Laocharoensuk, R.; Klimov, V. I.; Hollingsworth, J. A.; Htoon, H. 'Giant' CdSe/CdS Core/Shell Nanocrystal Quantum Dots As Efficient Electroluminescent Materials: Strong Influence of Shell Thickness on Light-Emitting Diode Performance. *Nano Lett.* **2011**, *12* (1), 331.
(31) Caruge, J. M.; Halpert, J. E.; Wood, V.; Bulovic, V.; Bawendi, M. G. Colloidal quantum-dot light-emitting diodes with metal-oxide charge transport layers. *Nature Photon.* **2008**, *2* (4), 247.
(32) Hikmet, R. A. M.; Talapin, D. V.; Weller, H. Study of conduction mechanism and electroluminescence in CdSe/ZnS quantum dot composites. *J. Appl. Phys.* **2003**, *93*, 3509.
(33) Bae, W. K.; Park, Y.-S.; Lim, J.; Lee, D.; Padilha, L. A.; McDaniel, H.; Robel, I.; Lee, C.; Pietryga, J. M.; Klimov, V. I. Controlling the influence of Auger recombination on the performance of quantum-dot light-emitting diodes. *Nat. Commun.* **2013**, 4.
(34) Mashford, B. S.; Stevenson, M.; Popovic, Z.; Hamilton, C.; Zhou, Z.; Breen, C.; Steckel, J.; Bulovic, V.; Bawendi, M.; Coe-Sullivan, S.; Kazlas, P. T. High-efficiency quantum-dot light-emitting devices with enhanced charge injection. *Nat. Photonics* **2013**, *7* (5), 407.
(35) Kwak, J.; Bae, W. K.; Lee, D.; Park, I.; Lim, J.; Park, M.; Cho, H.; Woo, H.; Yoon, D. Y.; Char, K.; Lee, S.; Lee, C. Bright and Efficient Full-Color Colloidal Quantum Dot Light-Emitting Diodes Using an Inverted Device Structure. *Nano Lett.* **2012**.
(36) Bozyigit, D.; Yarema, O.; Wood, V. Origins of Low Quantum Efficiencies in Quantum Dot LEDs. *Adv. Funct. Mater.* **2013**, *23* (24), 3024.
(37) Shirasaki, Y.; Supran, G. J.; Tisdale, W. A.; Bulović, V. Origin of Efficiency Roll-Off in Colloidal Quantum-Dot Light-Emitting Diodes. *Phys. Rev. Lett.* **2013**, *110* (21), 217403.
(38) Galland, C.; Ghosh, Y.; Steinbruck, A.; Sykora, M.; Hollingsworth, J. A.; Klimov, V. I.; Htoon, H. Two types of luminescence blinking revealed by spectroelectrochemistry of single quantum dots. *Nature* **2011**, *479* (7372), 203.
(39) Amelia, M.; Lincheneau, C.; Silvi, S.; Credi, A. Electrochemical properties of CdSe and CdTe quantum dots. *Chem. Soc. Rev.* **2012**, *41* (17), 5728.
(40) Brovelli, S.; Galland, C.; Viswanatha, R.; Klimov, V. I. Tuning Radiative Recombination in Cu-Doped Nanocrystals via Electrochemical Control of Surface Trapping. *Nano Lett.* **2012**, *12* (8), 4372.
(41) Galland, C.; Ghosh, Y.; Steinbrück, A.; Hollingsworth, J. A.; Htoon, H.; Klimov, V. I. Lifetime Blinking in Nonblinking Nanocrystal Quantum Dots. *Nat. Commun.* **2012**, *3*, 908.
(42) Yu, D.; Wang, C.; Guyot-Sionnest, P. n-Type Conducting CdSe Nanocrystal Solids. *Science* **2003**, *300* (5623), 1277.
(43) Kang, M. S.; Sahu, A.; Norris, D. J.; Frisbie, C. D. Size-Dependent Electrical Transport in CdSe Nanocrystal Thin Films. *Nano Lett.* **2010**, *10* (9), 3727.
(44) Jha, P. P.; Guyot-Sionnest, P. Trion Decay in Colloidal Quantum Dots. *ACS Nano* **2009**, *3* (4), 1011.
(45) Bae, W. K.; Brovelli, S.; Klimov, V. I. Spectroscopic Insights into the Performance of Quantum Dot Light Emitting Diodes. *MRS Bull.* **2013**, *38*, 721.
(46) Koh, W.-k.; Koposov, A. Y.; Stewart, J. T.; Pal, B. N.; Robel, I.; Pietryga, J. M.; Klimov, V. I. Heavily doped n-type PbSe and PbS nanocrystals using ground-state charge transfer from cobaltocene. *Sci. Rep.* **2013**, 3.
(47) Liu, F.; Biadala, L.; Rodina, A. V.; Yakovlev, D. R.; Dunker, D.; Javaux, C.; Hermier, J.-P.; Efros, A. L.; Dubertret, B.; Bayer, M. Spin dynamics of negatively charged excitons in CdSe/CdS colloidal nanocrystals. *Phys. Rev. B* **2013**, *88* (3), 035302.
(48) Park, Y. S.; Malko, A. V.; Vela, J.; Chen, Y.; Ghosh, Y.; García-Santamaría, F.; Hollingsworth, J. A.; Klimov, V. I.; Htoon, H. Near-Unity Quantum Yields of Biexciton Emission from CdSe/CdS Nanocrystals Measured Using Single-Particle Spectroscopy. *Phys. Rev. Lett.* **2011**, *106* (18), 187401.
(49) Yang, Y. A.; Wu, H.; Williams, K. R.; Cao, Y. C. Synthesis of CdSe and CdTe Nanocrystals without Precursor Injection. *Angew. Chem., Int. Ed.* **2005**, *44* (41), 6712.
(50) McGuire, J. A.; Sykora, M.; Joo, J.; Pietryga, J. M.; Klimov, V. I. Apparent Versus True Carrier Multiplication Yields in Semiconductor Nanocrystals. *Nano Lett.* **2010**, *10* (6), 2049.